A CCD Camera-based Hyperspectral Imaging System for Stationary and Airborne Applications

Chenghai Yang, James H. Everitt and **Michael R. Davis**
USDA-ARS, Kika de la Garza Subtropical Agricultural Research Center
2413 E. Highway 83, Weslaco, Texas 78596, USA
E-mail: cyang@weslaco.ars.usda.gov

Chengye Mao
ITD/Spectral Visions
Stennis Space Center, Mississippi, 39529, USA

Abstract

This paper describes a CCD (charge coupled device) camera-based hyperspectral imaging system designed for both stationary and airborne remote sensing applications. The system consists of a high performance digital CCD camera, an imaging spectrograph, an optional focal plane scanner, and a PC computer equipped with a frame grabbing board and camera utility software. The CCD camera provides 1280(h) x 1024(v) pixel resolution and true 12-bit dynamic range. The imaging spectrograph is attached to the camera via an adapter to disperse radiation into a range of spectral bands. The effective spectral range resulting from this integration is from 457.2 nm to 921.7 nm. The optional focal plane scanner can be attached to the front of the spectrograph via another adapter for stationary image acquisition. The camera and the frame grabbing board are connected via a double coaxial cable, and the utility software allows for complete camera control and image acquisition. The imaging system captures one line image for all the bands at a time and an aircraft or the focal plane scanner serves as a mobile platform to carry out pushbroom scanning in the along-track direction. The horizontal and vertical binning capability of the camera makes it possible to obtain images with various spatial (160, 320, 640 and 1280 pixels in image width) and spectral (32, 64, 128, 256, 512 and 1024 bands) resolutions. Formulas are presented to show the relationships among binning factors, spatial resolutions, and flight height and speed. Images with all 24 possible combinations of binning factors were collected in a laboratory setting. Airborne images with 128 bands and a width of 640 pixels were also obtained from agricultural fields, rangelands and waterways. Procedures were developed to correct geometric distortions of the airborne hyperspectral imagery. Preliminary image acquisition testing trials indicate that this CCD camera-based hyperspectral imaging system has potential for agricultural and natural resources applications.

Introduction

Use of hyperspectral remote sensing in both research and operational applications has been steadily increasing in the last decade. Hyperspectral imaging systems can capture imagery from tens to hundreds of narrow bands in the visible to infrared spectral regions. These systems offer new opportunities for better differentiation and estimation of biophysical attributes and have the potential for identification of optimal bands and/or band combinations for a variety of remote sensing applications. Many airborne hyperspectral sensors, including CASI (Anger, 1999), AVIRIS (Roberts *et al*., 1997), HYDICE (Willis *et al*., 1998), TRWIS (Winter *et al*., 1999), MIVIS (Bianchi *et al*., 1999), DAIS (Holmgren, 1999), and ASIA (Bars *et al*., 1999), have been deployed in various research projects and commercial applications. These systems employ aircraft as a platform for pushbroom scanning in the along track direction. A raw hyperspectral image cube is formed by a collection of scanned lines with all the bands. Since the stability of the platform is affected by the surrounding turbulent atmosphere during image acquisition, variations in altitude, attitude, and velocity will cause geometric distortions on the hyperspectral image (Gregory *et al*., 1999). Despite the significant progress in airborne hyperspectral remote sensing, hyperspectral imagery has not been used as widely as multispectral imagery partially due to the high costs of data acquisition and the geometric distortion of the imagery.

Recent advances in CCD cameras, frame grabber boards, and modular optical components have made it possible to assemble hyperspectral imaging sensors with off-the-shelf electronics. Sun *et al*. (1995) developed a spectrally filtered airborne video hyperspectral system by fitting linear variable interference filters onto two video CCD cameras. Mao *et al*. (1997) and Mao (1999) developed several prototype hyperspectral imaging systems using low cost digital CCD cameras and different types of hyperspectral imaging filters, including linear variable filters, prism-grating-prism (PGP)

spectrographs, and tunable wavelength filters. The integration of a PGP spectrograph and a focal plane scanner is an innovative approach to airborne and laboratory pushbroom hyperspectral imaging (Mao, 1999, 2000). The hyperspectral focal plane scanner scans an input image within the focal plane of a front lens to accomplish the task of pushbroom scanning, while the PGP spectrograph disperses an input line image vertically, as a function of the spectral wavelengths, and focuses a two dimensional output spectral matrix onto the sensor surface of a CCD camera. This integration eliminates the need for a mobile platform for ground and laboratory data acquisition and allows the imaging system to be used for both airborne and laboratory applications. Through a research agreement, ITD/Spectral Visions at Stennis Space Center, Mississippi, developed a CCD camera-based hyperspectral imaging system for research use at the USDA-ARS Kika de la Garza Subtropical Agricultural Research Center at Weslaco, Texas. This paper describes the hyperspectral imaging system and demonstrates with sample imagery its potential for agricultural and natural resources applications.

System Description

Figure 1 shows an airborne configuration (a) and a stationary configuration (b) of the hyperspectral imaging system. The airborne configuration consists of a digital camera, an imaging spectrograph and a front lens, while the stationary configuration has an additional focal plane scanner attached between the imaging spectrograph and the front lens on the basis of the airborne configuration. In either case, a personal computer equipped with a frame grabbing board and camera utility software is used for camera control and image acquisition. The camera is a SensiCam high performance digital CCD camera sensitive in the 280 to 1000 nm spectral range (The Cooke Corporation Ltd., Auburn Hills, MI). It is equipped with a cooled scientific grade SuperVGA CCD sensor that has 1280(h) × 1024(v) light-sensitive pixels. A 12-bit A/D converter built in the camera provides digital count values in the range of 0 to 4095. Other characteristics of the camera include its 12.5 MHz readout frequency, its pixel binning capability in both horizontal and vertical directions, and its wide range of selectable exposure time. Table 1 shows the major specifications for the camera.

The imaging spectrograph is the OEM (original equipment manufacturer) version of a PGP-based ImSpector V9 model with a 25 μm slit (Spectral Imaging Ltd., Oulu, Finland). The ImSpector is connected to the camera via a C-mount and an adapter to disperse the light passing through the entrance slit into a range of spectral bands. When radiation enters the spectrograph through the slit, it is collimated by a collimator lens and then dispersed at the PGP. Spatial information on the entrance slit is transferred to the CCD sensor at the horizontal axis (long axis) parallel to the slit length direction, while the spectrum is formed at the vertical axis (short axis) perpendicular to the horizontal axis. The effective spectral range resulting from this integration is from 457.2 nm to 921.7 nm. For the airborne configuration of the hyperspectral imaging system, a Xenoplan 1.4/17 mm compact lens (Schneider Optics, Inc., Hauppauge, NY) is directly connected to the spectrograph via a C-mount. An aircraft is needed to perform pushbroom scanning for this configuration. For the laboratory configuration, the focal plane scanner is attached to the front of the spectrograph via an adapter and the front lens is attached to the focal plane scanner via a C-mount. A CMA-12CC linear actuator (Newport Corporation, Irvine, CA) is used to drive the focal plane scanner either manually by an operator or automatically by a computer via a serial port. The linear actuator provides a wide range of speed with precision motion. The focal plane scanner performs line scanning across an input imaging area within the focal plane of the front lens and the spectrograph disperses each line into a spectrum and projects a two-dimensional image profile (line image) onto the CCD surface. This configuration allows image acquisition under stationary or laboratory settings. It can also be used for airborne applications to compensate the forward motion of the airborne platform to increase the along-track spatial resolution.

The computer is an Intel Pentium III (550 MHz) processor-based system with 768 MB of RAM and a 54 GB hard drive. The operating system on the computer is Microsoft Windows NT 4.0. A PCI interface board provided with the SensiCam imaging system is installed in a master PCI slot in the computer. The SensiControl utility software supplied with the camera is installed in the computer for complete camera control and image acquisition. The camera is connected to the PCI interface board via a double coaxial cable. The control parameters for the camera such as exposure time, horizontal and vertical binning factors can be set before image acquisition. There are four horizontal binning factors (1, 2, 4, and 8) and six vertical binning factors (1, 2, 4, 8, 16, and 32) from which to choose. Horizontal binning determines the across-track width of the image, while vertical binning determines the number of spectral bands. For example, a horizontal binning factor of 1 and a vertical binning factor of 1 will provide a full spatial resolution of 1280 pixels in image width and a maximum of 1024 spectral bands for the

Table 1 Major specifications for a high performance digital CCD camera.

Camera type	Super VGA SensiCam
Sensor type	CCD-interline progressive scan
Number of pixel	1280(h) × 1024(v)
Pixel size	6.7μm × 6.7μm
Sensor format	2/3”
Scan area	8.6mm × 6.9mm
Scan rate	12.5MHz
Dynamic range	12 bit(0-4095)
Spectral response	280-1000mm
Horizontal binning	1, 2, 4, 8
Vertical binning	1, 2, 4, 8, 16, 32
Exposure time	1ms-1000s

Figure 1 Airborne configuration (a) and stationary configuration (b) of a hyperspectral imaging system. The main components of the system include a SensiCam digital CCD camera (A), an imaging spectrograph (B), a front lens (C), and an optional focal plane scanner (D).

CCD camera, while a horizontal binning factor of 2 and a vertical binning factor of 8 will reduce the spatial resolution to 1280/2=640 pixels and the number of spectral bands to 1024/8=128. Binning is a very useful tool in an imaging system because it gives the flexibility to obtain imagery with various spatial and spectral resolutions. Moreover, binning can effectively increase the sensor's sensitivity to light by combining adjacent pixels and reduce the size of the image for fast acquisition.

The imaging system captures one line image with all the bands at a time. Each line image consists of up to 1280 pixels in the across-track dimension and each pixel contains up to 1024 bands. The PCI interface board gets the 12 bit data from the camera and transfers them via PCI-Bus to a 16 bit data array of the computer's RAM (the higher 4 bits are set to zero). The frame rate, or the number of line images that can be captured in one second, depends on the settings of horizontal and vertical binning and exposure time. Generally, the larger the binning factors and/or the shorter the exposure time, the higher the frame rate. However, the total number of line images that can be captured continuously at one time depends on the size of each line image and the RAM available in the computer because all the line images are stored temporarily in the RAM before being stored in the hard drive. When the SensiControl software is running, the maximum available RAM for image storage is approximately 500 MB in this particular computer. Table 2 summarizes the image width in pixels, number of spectral bands, CCD readout time, frame rate, and maximum number of line images that can be stored in the computer's RAM at one time for all horizontal and vertical binning combinations of the hyperspectral imaging system. If the exposure time is set shorter than the readout time, the specified frame rate can be obtained. Otherwise, the frame rate depends on the duration of the set exposure time. For example, for a horizontal binning factor of 2 and a vertical binning factor of 8, frame rate can be as fast as 31.58 line images per second at an exposure time of 31.67 ms or less, while the maximum number of line images that can be stored in the RAM is 3236. The line images captured in the RAM can be saved

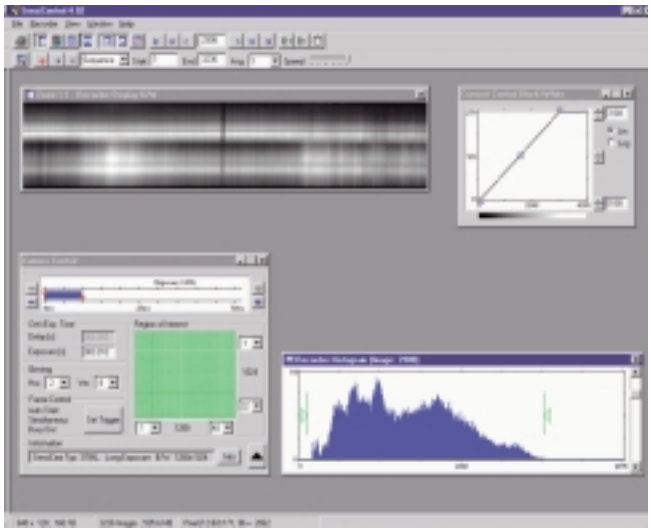

Figure 2 A screen capture of a line image with 640 pixels in the horizontal direction and 128 bands in the vertical direction. Also shown are the control panel with the camera settings, the convert control from 12 bit data into 8 bit data, and a histogram of the line image.

onto the computer's hard drive in individual B16 files. A B16 file consists of header information (128 bytes) and the 16 bit pixel values (2 bytes each) for each line image. All the B16 files captured from one field or area in a pushbroom operation can be combined to form a three-dimensional hyperspectral image or cube. After the line images stored in the RAM are saved to the hard drive, a new set of line images can be captured. The software can also display a line image on the computer's monitor by automatically converting the 12 bit data to 8 bit data. Figure 2 shows a screen capture of a line image with 640 pixels in the horizontal direction and 128 bands in the vertical direction. Also shown in the figure are the control panel with the camera settings, the convert control from 12 bit data into 8 bit data, and a histogram of the line image.

Since the hyperspectral imaging system captures one line image with all the bands at a time along the pushbroom

Table 2 Image width, number of spectral bands, CCD readout time, frame rate, and maximum number of line images that can be stored in the computer's RAM at one time for all horizontal and vertical binning combinations of the hyperspectral imaging system.

Horizontal binning	Vertical binning	Image width (pixels)	Spectral bands	Readout time (ms)	Frame rate (images/s)	Maximum line images
1	1	1280	1024	121.74	8.21	201
1	2	1280	512	61.69	16.21	403
1	4	1280	256	61.69	16.21	808
1	8	1280	128	31.67	31.58	1617
1	16	1280	64	16.65	60.05	3236
1	32	1280	32	12.90	77.51	6474
2	1	640	1024	121.74	8.21	403
2	2	640	512	61.69	16.21	808
2	4	640	256	61.69	16.21	1617
2	8	640	128	31.67	31.58	3236
2	16	640	64	16.65	60.05	6474
2	32	640	32	12.90	77.51	9999
4	1	320	1024	121.74	8.21	808
4	2	320	512	61.69	16.21	1617
4	4	320	256	61.69	16.21	3236
4	8	320	128	31.67	31.58	6474
4	16	320	64	16.65	60.05	9999
4	32	320	32	12.90	77.51	9999
8	1	160	1024	121.74	8.21	1617
8	2	160	512	61.69	16.21	3236
8	4	160	256	61.69	16.21	6474
8	8	160	128	31.67	31.58	9999
8	16	160	64	16.65	60.05	9999
8	32	160	32	12.90	77.51	9999

scanning direction, the two-dimensional line image gives very little information about the geometric view of the imaging area. This creates some difficulty for the operator to see if a correct field or area is being imaged. Therefore, a three-camera imaging system described by Escobar *et al*. (1997) is used as a view finder to locate the target. The system is composed of three noninterlaced Kodak Megaplus digital CCD cameras and a computer equipped with three image digitizing boards that have the capability of obtaining scene frames with 1024 by 1024 pixels. The cameras are filtered for spectral observations in the visible green (555-565 nm), red (625-635 nm), and near-infrared (NIR) (845-857 nm) bands. The color-infrared (CIR) composite images taken by the three-camera system can be used as normal multispectral imagery and also as references for geometric correction of hyperspectral images. Since the Megaplus and the SensiCam have similar sensor areas, to ensure both imaging systems provide similar ground coverage along the across-track direction, the lenses attached to the Megaplus cameras have the same focal length (17 mm) as that for the SensiCam. The SensiCam is mounted and aligned with the three Megaplus cameras on a light aluminum frame as shown in Figure 3.

Relationships among Camera Parameters, Spatial Resolutions, and Flight Height and Speed

The hyperspectral imaging system can simultaneously capture hyperspectral data for an entire line in the across-track direction without any mechanical movement, but it requires a mobile platform such as an aircraft or the focal plane scanner to carry out the pushbroom scanning in the along-track direction. The speed of the mobile platform will determine the number of lines captured in the along-track direction within a given time period or travel distance for a given binning combination. The faster the mobile platform moves, the fewer lines are captured. As shown in Table 2, regardless of platform speed, the imaging system can acquire anywhere from 8.21 to 77.51 lines per second for various horizontal and vertical binning combinations. Therefore, appropriate platform speed has to be determined so that there is a certain amount of forward overlap between successive lines.

The width of the scan line, or the spatial resolution, in the along-track direction is defined by the width of the slit (25μm) on the imaging spectrograph, while the spatial

resolution in the across-track direction is determined by the sensor's pixel size (6.7μm) and horizontal binning factors (1, 2, 4 and 8). For example, the pixel dimension in terms of sensor area is 6.7μm × 25μm for a horizontal binning factor of 1 and 13.4μm × 25μm for a horizontal binning factor of 2. For a focal length of 17 mm and a flight height of 1000 m, the ground pixel dimension is 0.788m × 1.471m for a horizontal binning factor of 2, that is, each pixel covers 0.788m in the across-track direction and 1.471m in the along-track direction. Therefore, to prevent forward gaps, platform speed should be so determined that the distance between any two successive lines is no more than 1.471m at a flight height of 1000 m. If square pixels are required for the image, the forward overlap should be 1.471-0.788=0.683 m or 46.4%. That means that the distance between successive lines is the same as the pixel size in the across-track direction. It should be noted that forward overlap will reduce the effective pixel size in the along-track direction, but will not change the spatial resolution in this direction. In other words, although the effective pixel size in the along-track direction is 0.788 m with a forward overlap of 46.4%, but the spatial resolution in this direction is still 1.471 m, the same as the width of the scan line.

Generally, the line width on ground in the along-track direction (W_s), the ground pixel size in the across-track direction (G_h), and the ground pixel size in the along-track direction (G_v) are determined by

$$W_s = \frac{SH}{1000F}, \tag{1}$$

$$G_h = \frac{PB_hH}{1000F}, \tag{2}$$

and

$$G_v = \frac{5V}{18R}, \tag{3}$$

where S is entrance slit (μm), H is flight height above ground (m), and F is focal length (mm), P is sensor's pixel size (μm), B_h is horizontal binning factor, V is airplane velocity (km/h), and R is frame rate (line images per second). To avoid forward skip, the pixel size in the along-track direction should be less than or equal to the line width, that is, $G_v \le W_s$. From Eqs. (1) and (3), aircraft velocity and flight height should meet the following condition:

$$V \le \frac{9SHR}{2500F}, \tag{4}$$

To have square pixels, the pixel size in the across-track direction should be equal to the pixel size in the along-track direction, that is, $G_h = G_v$. From Eqs. (2) and (3), we have

$$V = \frac{9PB_hHR}{2500F}, \tag{5}$$

Since aircraft speed determined from Eq. (5) has to meet condition (4), we have

$$B_h \le \frac{S}{P}, \tag{6}$$

Therefore, only if condition (6) is met can square pixels be achieved. Otherwise, the pixel size in the along-track direction will be smaller than that in the across-track direction. Since S = 25 μm and P = 6.7 μm for this particular system, we have $B_h \le 3.73$. Thus only when horizontal binning is 1 or 2 can square pixels be obtained. When horizontal binning is 4 or 8, the pixel size in the along-track direction has to be smaller than that in the across-track direction to avoid forward skip. In reality, it is not necessary to obtain images with square pixels because images will be resampled to square pixels during the georeferencing procedure. Even if aircraft speed and flight height are so determined for square pixels, the actual pixels won't be perfectly square because the actual speed and height do vary slightly. Using formulas (1)-(6), aircraft velocity and flight height as well as pixel sizes can be determined for any given camera parameters. As an example, Table 3 shows aircraft velocity required for acquiring images with square pixels at various altitudes for a horizontal binning factor of 2 and a vertical binning factor of 8.

Stationary and Airborne Image Acquisition

The stationary configuration of the hyperspectral imaging system was used to take images of the natural scenery outside a building for all 24 horizontal and vertical binning combinations. The camera was positioned horizontally so that the grass, trees, sky, and other objects within the field of view could be captured. The scanning speed of the focal plane scanner was first manually determined and then maintained constantly during pushbroom scanning for each binning combination. Figure 4a shows a CIR composite image extracted from a 128-band hyperspectral cube with a width of 640 pixels and a height of 630 pixels, while Figure 4b shows a CIR image derived from a 64-band hyperspectral image with a width of 1280 pixels and a height of 1200 pixels. For the 128-band image, the center wavelengths for the NIR, red and green bands were 850.0, 628.7, and 559.7 nm, respectively, and the band width was 3.63 nm. For the 64-band image, the center wavelengths for the NIR, red and green bands were 848.2, 630.5, and 557.9 nm, respectively, and the band width was 7.26 nm. Both images show the objects, such as palm trees, grass, shadows, the concrete pipe and the sky, within the imaging area in distinct colors. Although band width and pixel size are different between the two images, both look much alike. Only when the images are magnified can differences in spatial resolution be seen between the two.

A Cessna 206 single-engine aircraft was used as the platform for airborne image acquisition testing. The airborne configuration of the hyperspectral imaging system and the three-camera system were installed on the aircraft. Since no stabilizer or inertial measurement device was used to damper or measure platform variations, care was taken to minimize the effects of winds and changes in the aircraft's speed and

flight direction. The aircraft was stabilized at the predetermined altitude, speed and flight direction before the start of image acquisition and was maintained at the same altitude, speed and direction during the course of pushbroom scanning. For the year 2000 testing, a horizontal binning of 2 and a vertical binning of 8 were used to obtain 128-band images with 640 pixels in width. Hyperspectral images were acquired under sunny and calm conditions from agricultural fields, rangelands, and waterways in south Texas. Flight height was set at 1676 m (5500 ft) and flight speed was set 150 km/h (93 mi/h) to acquire images with square pixels (Table 3). Figures 5a, 6a and 7a show three CIR image derived from three raw (uncorrected) 128-band hyperspectral images obtained from a grain sorghum field, a rangeland area, and a section of the Arroyo Colorado river in south Texas, respectively. The center wavelengths for the NIR, red and green bands for the three color composites were 850.0, 628.7, and 559.7 nm, respectively, and the band width was 3.63 nm. Despite the efforts to minimize the effects of the aircraft's motions during image acquisition, obvious distortions can be seen in the three images.

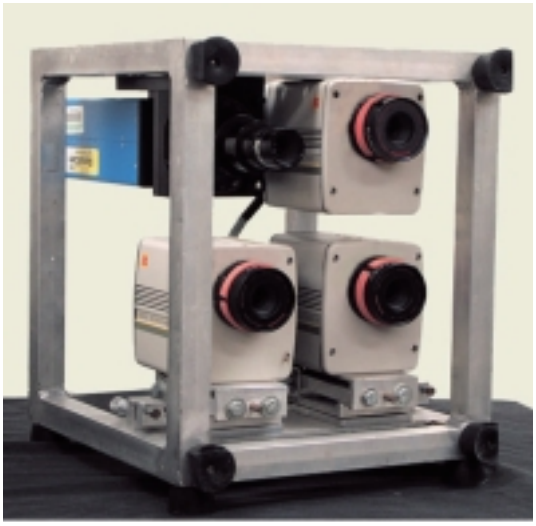

Figure 3 A SensiCam hyperspectral camera mounted and aligned with three Megaplus multispectral cameras on a light aluminum frame.

A moving aircraft has six degrees of freedom, that is, speed changes in the along-track direction, movements in the across-track direction, variations in altitude, pitch, roll, and yaw. The distortions seen on the images were mainly due to movements in the across-track direction and variations in roll. For instance, the highway and the dirt road on both sides of the grain sorghum field were supposed to be straight, but they became wiggly lines on the image. These distortions can be corrected by shifting each line in the across-track direction to a reference line (e.g., the highway or dirt road) so that the highway and dirt road become straight on the corrected image. Variations in speed, altitude, pitch, and yaw also affected the quality of the image, though these effects could hardly be seen on the image visually. These distortions were hidden in the image and were more difficult to correct. However, change in altitude had very little effect on the image because of the high flight altitude.

Procedures were developed based on a reference line method to correct the distortions in the across-track direction. A reference line approximately parallel to the flight line was first identified and overlaid on the corresponding distorted line on the raw image. Then the distances in pixels between the reference line and the distorted line were calculated for each row of the raw image. Finally, each row was shifted in the across-track direction by the number of pixels determined. These procedures were implemented by

(a) 640 × 630 (b) 1280 × 1200

Figure 4 A CIR image extracted from a 128-band hyperspectral image (a) and a CIR image extracted from a 64-band hyperspectral image (b). For the 128-band image, the center wavelengths for the NIR, red and green bands were 850.0, 628.7, and 559.7 nm, respectively, and the band width was 3.63 nm. For the 64-band image, the center wavelengths for the NIR, red and green bands were 848.2, 630.5, and 557.9 nm, respectively, and the band width was 7.26 nm.

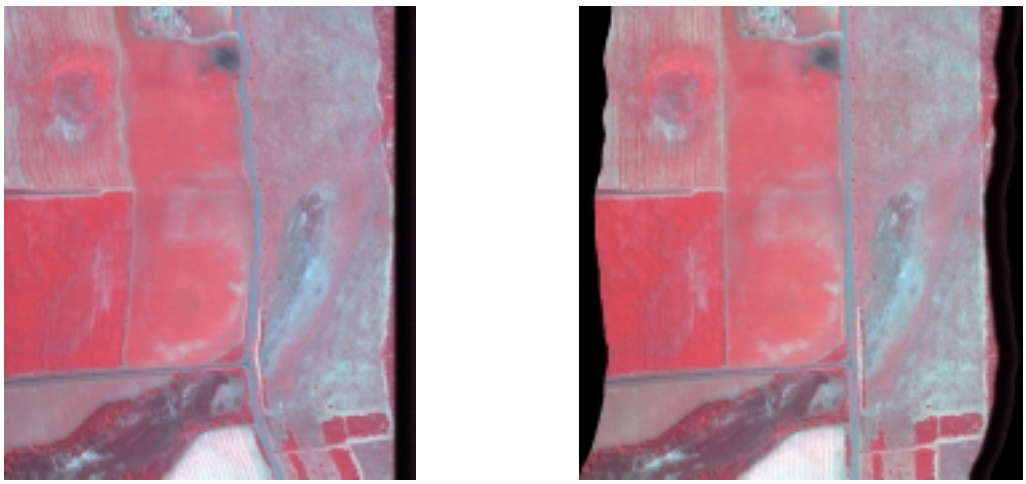

(a) Raw CIR image (640 × 740)

(b) Corrected CIR image (691 × 740)

Figure 5 A raw CIR image (a) and a corrected CIR image (b) for a grain sorghum field in south Texas. These images were extracted from a raw 128-band hyperspectral image and its corrected version, respectively. The center wavelengths for the NIR, red, and green bands were 850.0, 628.7, and 559.7 nm, respectively, and the band width was 3.63 nm.

Table 3 Line width, ground pixel size, and aircraft speed required for square pixels at different altitudes for a hyperspectral imaging system.

Flight height		Aircraft velocity		Line width	Pixel size	Across-track coverage
(ft)	(m)	(mi/h)	(km/h)	(m)	(m)	(m)
2000	610	34	55	0.896	0.481	308
2500	762	42	68	1.121	0.601	384
3000	914	51	82	1.345	0.721	461
3500	1067	59	96	1.569	0.841	538
4000	1219	68	109	1.793	0.961	615
4500	1372	76	123	2.017	1.081	692
5000	1524	85	137	2.241	1.201	769
5500	1676	93	150	2.464	1.321	846
6000	1829	102	164	2.689	1.442	923
6500	1981	110	178	2.914	1.562	999
7000	2134	119	191	3.138	1.682	1076
7500	2286	127	205	3.362	1.802	1153
8000	2438	136	219	3.586	1.922	1230

The calculated values on the table are based on the following parameters: slit=25µm, sensor's pixel size=6.7µm, horizontal binning factor=2, vertical binning factor=8, across-track image size=640 pixels, along-track image size<=3236 pixels, number of spectral bands=128, frame rate=31.58 line images/s, exposure time <=31 ms, focal length=17mm.

using ERDAS IMAGINE, ArcInfo, and programs developed at the USDA-ARS Research Center at Weslaco, Texas. Figure 5b shows a CIR image composite extracted from a corrected version of the 128-band hyperspectral image for the field. The image clearly reveals spatial plant growth variability within the field. The center wavelengths and band width for the NIR, red and green bands used in the composite image were the same as those for Figure 5a. Clearly, the highway and the dirt road look straight on the corrected image. This approach involves no image resampling and therefore preserves the original radiometric values of the image. The procedure is successful if a reference line approximately parallel to the flight line exists in the image. This may not be a problem for some agricultural applications because field boundaries can be found in most agricultural fields. The same procedures were applied to the image for the rangeland area since there is a straight fence line in the along-track direction. Figure 6b shows a CIR image derived from the corrected version of the 128-band hyperspectral image for the rangeland area. Major

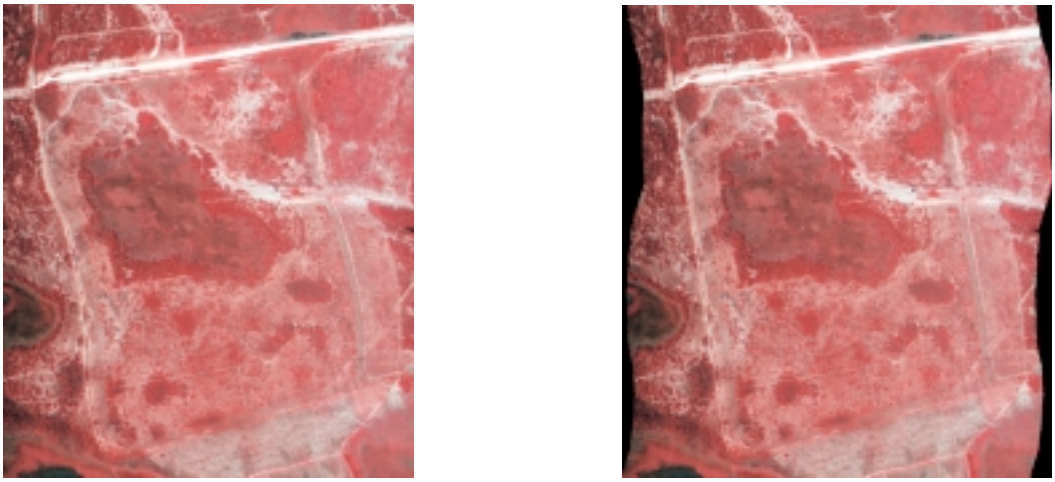

(a) Raw CIR image (640 × 740) (b) Corrected CIR image (676 × 740)

Figure 6 A raw CIR image (a) and a corrected CIR image (b) for a rangeland area in south Texas. These images were extracted from a raw 128-band hyperspectral image and its corrected version, respectively. The center wavelengths for the NIR, red, and green bands were 850.0, 628.7, and 559.7 nm, respectively, and the band width was 3.63 nm.

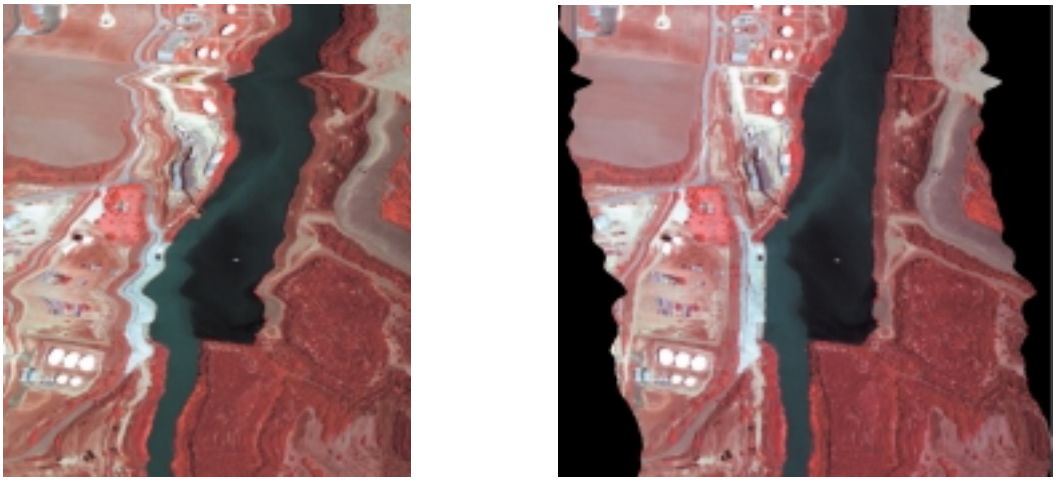

(a) Raw CIR image (640 × 740) (b) Corrected CIR image (676 × 740)

Figure 7 A raw CIR image (a) and a corrected CIR image (b) for a section of the Arroyo Colorado river in south Texas. These images were extracted from a raw 128-band hyperspectral image and its corrected version, respectively. The center wavelengths for the NIR, red, and green bands were 850.0, 628.7, and 559.7 nm, respectively, and the band width was 3.63 nm.

land cover types such as mixed brush and grass, dry soil and roads, and wet areas can be distinguished in the image.

In many natural resources applications, a reference line may not exist in the imaging area. The image shown in Figure 7a is one example. Therefore, another approach based on maximized correlations between successive lines (rows) was developed to correct the image distortion in the across-track direction. This approach assumed that any shift of a successive scan line relative to the preceding scan line along the across-track direction will reduce the correlation between the two lines. Computer programs were developed to determine the optimal number of pixels to be shifted between any two successive scan lines and to shift each line by the determined number of pixels along the across-track direction. Similarly, this approach does not involve resampling and maintains original image values. Figure 7b shows a CIR composite derived from the corrected version of the 128-band hyperspectral image for the section of the river. Figure 8 shows four individual band images extracted from the corrected 128-band hyperspectral image for the section of the river. The center wavelengths for the NIR, red, green, and blue bands were 850.0, 628.7, 559.7, and 487.2 nm, respectively, and the band width was 3.63 nm. These images highlight the water

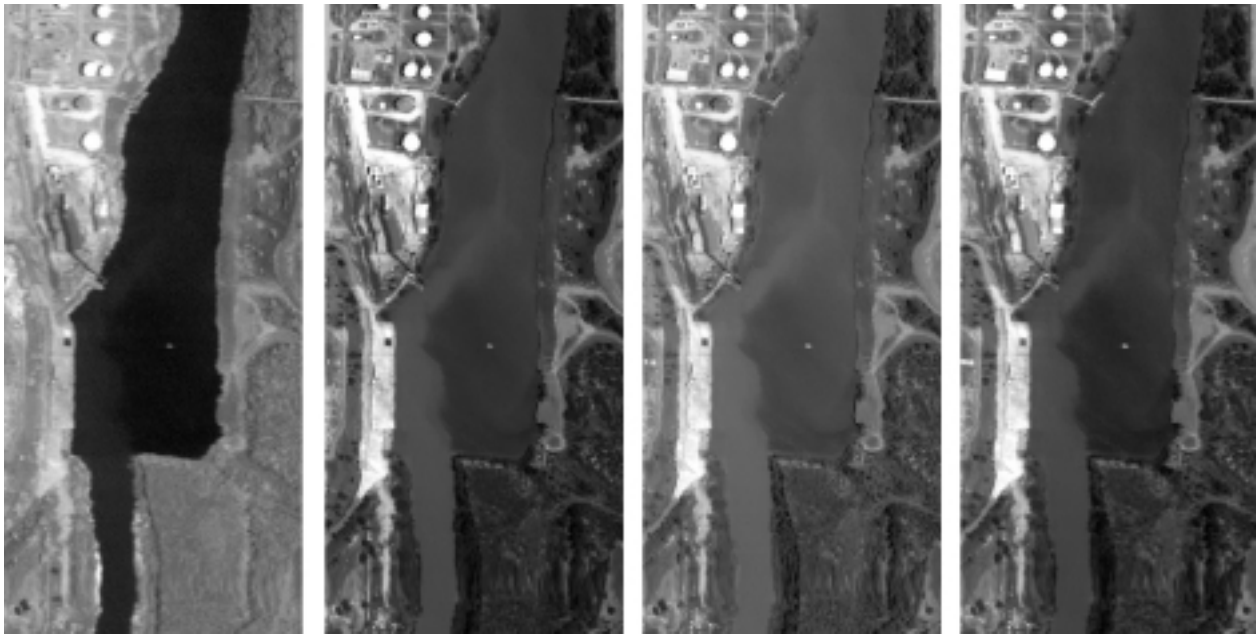

(a) NIR band (b) Red band (c) Green band (d) Blue band

Figure 8 Band images extracted from a corrected 128-band hyperspectral image for a section of the Arroyo Colorado river in south Texas. The center wavelengths for the NIR, red, green, and blue bands were 850.0, 628.7, 559.7, and 487.2 nm, respectively, and the band width was 3.63 nm.

pollution problems caused by municipal, industrial and agricultural discharges; however, the band images reveal that the visible bands can better detect the effluents than the NIR band. As can be seen, the distorted circular tanks and the concrete dock in the image were almost restored, but minor distortion remains. This is because this approach does not guarantee that features with known geometric shapes, such as straight lines and circles, on the imaging area will be preserved after correction. Therefore, joint use of the two approaches may enhance the accuracy of geometric correction if reference lines or features with known geometric shapes can be found in the imaging scenes.

Conclusions

The CCD camera-based hyperspectral imaging system described in this paper shows promise for agricultural and natural resources applications. It can be a useful remote sensing tool as the trend toward increased use of cost-effective airborne hyperspectral imaging systems continues. One unique feature of the hyperspectral imaging system is that it can be used for both stationary and airborne applications. The horizontal and vertical binning capability of the camera allows images with various spatial and spectral resolutions to be obtained. However, flight height and speed have to be carefully determined for each binning combination to achieve desired resolutions and ground coverage. The formulas presented in this paper can be used as a guidance for determining the camera and flight parameters before a flight mission. Geometric distortion is an inherited problem in imagery acquired from this system as from any other airborne pushbroom imaging system. Although developing techniques for geometric correction was not the main objective for this paper, the procedures presented in this paper can be used to correct much of the distortion caused by movements in the across-track direction and motions in roll. However, a six-degree of freedom measurement unit that provides accurate and instantaneous attitude and positional data at a high sampling rate should allow more distortions to be corrected. More research work is needed to evaluate the hyperspectral imaging system for both stationary and airborne remote sensing applications.

Acknowledgments

The authors wish to thank Juan Noriega, Fred Gomez, Buck Cavozos and Jim Forward for their assistance in the testing of the hyperspectral imaging system.

References

Anger, C. D. 1999. Airborne hyperspectral remote sensing in the future. Proc. 4th International Airborne Remote Sensing Conference and Exhibition/21st Canadian Symposium on Remote Sensing, ERIM International, Inc., Ann Arbor, MI. Vol. 1, pp. 1-5.

Bars, R., L. Watson, and O. Weatherbee. 1999. AISA as a tool for timely commercial remote sensing. Proc. 4th International Airborne Remote Sensing Conference and Exhibition/21st Canadian Symposium on Remote Sensing, ERIM International, Inc., Ann Arbor, MI. Vol. 1, pp. 239-246.

Bianchi, R., R. M. Cavalli, L. Fiumi, C. M. Marino, and S. Pignatti. 1999. Airborne MIVIS hyperspectral imaging spectrometer over natural and anthropic areas. Proc. 4th International Airborne Remote Sensing Conference and Exhibition/21st Canadian Symposium on Remote Sensing, ERIM International, Inc., Ann Arbor, MI. Vol. 1, pp. 337-344.

Escobar, D. E., J. H. Everitt, J. R. Noriega, M. R. Davis, and I. Cavazos. 1997. A true digital imaging system for remote sensing applications. Proc. 16th Biennial Workshop on Color Photography and Videography in Resource Assessment, American Society for photogrammetry and remote sensing, Bethesda, Maryland, pp. 470-484.

Gregory, S., P. Hedges, and J. Elgy. 1999. The geometric correction of airborne line-scanner imagery. Proc. 4th International Airborne Remote Sensing Conference and Exhibition/21st Canadian Symposium on Remote Sensing, ERIM International, Inc., Ann Arbor, MI. Vol. 1, pp. 178-185.

Holmgren, J., H. Olsson, J. Wallerman, S. Joyce, O. Hagner, J. Bergh, and S. Linder. 1999. Radiance over boreal forest stands in northern Sweden as measured by the 79 channel DAIS-7915 imaging spectrometer. Proc. 4th International Airborne Remote Sensing Conference and Exhibition/21st Canadian Symposium on Remote Sensing, ERIM International, Inc., Ann Arbor, MI. Vol. 1, pp. 212-219.

Mao, C. 1999. Hyperspectral imaging systems with digital CCD cameras for both airborne and laboratory application. Proc. 17th Biennial Workshop on Videography and Color Photography in Resource Assessment, American Society for Photogrammetry and Remote Sensing, Bethesda, MD. pp. 31-40.

Mao, C. 2000. Hyperspectral focal plane scanning-an innovative approach to airborne and laboratory pushbroom hyperspectral imaging. Proc. 2nd International Conference on Geospatial Information in Agriculture and Forestry, ERIM International, Inc., Ann Arbor, MI. Vol. 1, pp. 424-428.

Mao, C., M. Seal, and G. Heitschmidt. 1997. Airborne hyperspectral image acquisition with digital CCD video camera. Proc. 16th Binnial Workshop on Videography and Color Photography in Resource Assessment, American Society for Photogrammetry and Remote Sensing, Bethesda, MD. pp. 129-140.

Roberts, D. A., R. O. Green, and J. B. Adams. 1997. Temporal and spatial patterns in vegetation and atmospheric properties from AVIRIS. *Remote Sens. Environ*. 62: 223-240.

Sun, X., J. Baker, and R. Hordon. 1995. A spectrally-filtered airborne video system and its imagery. Proc. 15th Biennial Workshop on Color Photography and Videography in Resource Assessment, American Society for photogrammetry and remote sensing, Bethesda, MD. pp. 253-259.

Willis, P. R., P. G. Carter, and C. J. Johansen. 1998. Assessing yield parameters by remote sensing techniques. Proc. 4th International Conference on Precision Agriculture, pp. 1465-1473, ASA/CSSA/SSSA, Madison, WI.

Winter, E. M., M. J. Schlangen, and M. E. Winter. 1999. Comparison of techniques for the classification of vegetation using a hyperspectral sensor. Proc. 4th International Airborne Remote Sensing Conference and Exhibition/21st Canadian Symposium on Remote Sensing, ERIM International, Inc., Ann Arbor, MI. Vol. 1, pp. 723-728.